



<b>Title</b>	Experimental Demonstration of a Mode Shape-Based Scour-Monitoring Method for Multispan Bridges with Shallow Foundations
<b>Authors(s)</b>	Malekjafarian, Abdollah, Kim, Chul-Woo, O'Brien, Eugene J., Fitzgerald, Paul C., et al.
<b>Publication date</b>	2020-08
<b>Publication information</b>	Malekjafarian, Abdollah, Chul-Woo Kim, Eugene J. O'Brien, Paul C. Fitzgerald, and et al. "Experimental Demonstration of a Mode Shape-Based Scour-Monitoring Method for Multispan Bridges with Shallow Foundations." American Society of Civil Engineers (ASCE), August 2020. <a href="https://doi.org/10.1061/(asce)be.1943-5592.0001586">https://doi.org/10.1061/(asce)be.1943-5592.0001586</a> .
<b>Publisher</b>	American Society of Civil Engineers (ASCE)
<b>Item record/more information</b>	<a href="http://hdl.handle.net/10197/12040">http://hdl.handle.net/10197/12040</a>
<b>Publisher's statement</b>	This material may be downloaded for personal use only. Any other use requires prior permission of the American Society of Civil Engineers. This material may be found at <a href="https://ascelibrary.org/doi/10.1061/%28ASCE%29BE.1943-5592.0001586">https://ascelibrary.org/doi/10.1061/%28ASCE%29BE.1943-5592.0001586</a>
<b>Publisher's version (DOI)</b>	10.1061/(asce)be.1943-5592.0001586

Downloaded 2026-05-01 23:49:13

The UCD community has made this article openly available. Please share how this access benefits you. Your story matters! (@ucd\_oa)



© Some rights reserved. For more information

# 1 Experimental demonstration of a mode shape-based scour 2 monitoring method for multi-span bridges with shallow 3 foundations

4 Abdollah Malekjafarian, Ph.D. <sup>1</sup>, Chul-Woo Kim, Ph.D. <sup>2</sup>, Eugene J. OBrien, Ph.D. <sup>3</sup>,  
5 Luke J. Prendergast, Ph.D. <sup>4</sup>, Paul C. Fitzgerald, Ph.D. <sup>5\*</sup>, Syunsuke Nakajima <sup>6</sup>

## 6 **Abstract**

7 This paper experimentally investigates a vibration-based scour monitoring approach applicable  
8 to bridges with multiple simply supported spans on shallow foundations. A monitoring strategy  
9 based on the relative changes in pier mode shape amplitudes due to scour is postulated. The  
10 first global mode shape of a bridge structure with multiple spans is extracted from acceleration  
11 measurements using an output-only approach, Frequency Domain Decomposition (FDD). The  
12 relative changes of the pier mode shape amplitudes under scour are then tracked. Here, each  
13 pier mode shape value is compared with the mean values of the remaining piers in a process  
14 that creates a Mean-Normalised Mode Shape (MNMS). The approach is demonstrated on a  
15 scaled model of a bridge with four spans, supported on sprung foundations, where scour is  
16 simulated by the replacement of springs with springs of lower stiffness corresponding to a  
17 reduction in foundation stiffness. It is shown that at a given ‘scoured’ pier, significant increases  
18 in the MNMS value occur, suggesting that the location of the scour can be identified. The  
19 magnitude of the MNMS at a given pier also increases with an increase in stiffness loss due to  
20 scour. In practice, the approach would work best by carrying out a visual inspection of the

---

<sup>1</sup> School of Civil Engineering, University College Dublin, Dublin, Ireland. Email [abdollah.malekjafarian@ucd.ie](mailto:abdollah.malekjafarian@ucd.ie)

<sup>2</sup> Department of Civil and Earth Resources Engineering, Kyoto University, Kyoto 615-8540, Japan. Email [kim.chulwoo.5u@kyoto-u.ac.jp](mailto:kim.chulwoo.5u@kyoto-u.ac.jp)

<sup>3</sup> School of Civil Engineering, University College Dublin, Dublin, Ireland. Email [eugene.obrien@ucd.ie](mailto:eugene.obrien@ucd.ie)

<sup>4</sup> Department of Civil Engineering, Faculty of Engineering, University of Nottingham, Nottingham, NG7 2RD, United Kingdom. Email [luke.prendergast@nottingham.ac.uk](mailto:luke.prendergast@nottingham.ac.uk)

<sup>5</sup> School of Civil Engineering, University College Dublin, Dublin, Ireland. Email [paul.fitzgerald.3@ucdconnect.ie](mailto:paul.fitzgerald.3@ucdconnect.ie)

<sup>6</sup> Department of Civil and Earth Resources Engineering, Kyoto University, Kyoto 615-8540, Japan. Email [nakajima.syunsuke.35x@st.kyoto-u.ac.jp](mailto:nakajima.syunsuke.35x@st.kyoto-u.ac.jp)

\*Corresponding author

21 bridge to establish the initial health condition at the time of sensor installation. After this initial  
22 process, the bridge can be monitored remotely for scour on an ongoing basis.

23 **Keywords:** Bridge scour; accelerations; mode shape; damage detection; SHM; vibrations

## 24 **Introduction**

25 Scour erosion, where soil is removed from around bridge foundations by the action of flowing  
26 water (Hamill, 1999), remains a significant hazard to bridges worldwide (Wardhana and  
27 Hadipriono, 2003, Maddison, 2012, Prendergast et al., 2018). There are three main forms of  
28 scour, general, contraction and local. General scour occurs naturally in river channels and  
29 includes the aggradation and degradation of the river bed that may occur as a result of changes  
30 in the hydraulic parameters governing flow such as changes in the flow rate or changes in the  
31 quantity of sediment in the channel (Forde et al., 1999). Contraction scour occurs due to  
32 changes in the cross-sectional (flow) area of a river due to the presence of obstructions such as  
33 piers or abutments. Local scour occurs in the direct vicinity of a bridge foundation where  
34 downward flow is induced at the upstream end of bridge piers, leading to local erosion (Forde  
35 et al., 1999).

36 In its simplest form, scour leads to a lowering of the soil elevation relative to foundation  
37 elements of a bridge, which can increase the vulnerability to failure. Perhaps a more significant  
38 issue occurs for bridges founded on shallow pad foundations, where scour can undermine the  
39 pad, decreasing the soil-structure contact area. This leads to increased stress on the remaining  
40 soil, increasing soil strains and ultimately reducing the shear stiffness of the soil beneath the  
41 foundation system (Oztoprak and Bolton, 2013). This type of scour mechanism is particularly  
42 dangerous because many bridges have unknown foundation depths, meaning it is difficult for  
43 bridge owners/operators to truly understand scour risk (Briaud et al., 2012).

44 The reduction in foundation stiffness as a result of scour can lead to excessive settlements,  
45 which pose issues to bridges and can affect their load-carrying capacity. In terms of load-rating  
46 of structures to identify carrying capacity, recent efforts have sought to include foundation  
47 settlements into assessment frameworks (Davis et al., 2018).

48 It is widely recognised that scour reduces the stiffness of foundations, which has given rise to  
49 the area of vibration-based scour detection (Briaud et al., 2011, Foti and Sabia, 2010,  
50 Prendergast et al., 2013, Chen et al., 2014, Klinga and Alipour, 2015, Prendergast et al., 2016a,  
51 Xiong et al., 2018b, Kong et al., 2013, Fitzgerald et al., 2019a). The idea that changes in  
52 stiffness manifest themselves as changes to modal properties is the original concept behind  
53 monitoring dynamic properties for structural damage detection (Sohn et al., 2003). Many  
54 researchers have investigated approaches to scour detection based on measuring changes in  
55 various dynamic properties using sensors installed on the superstructure, or on passing vehicles  
56 (Fitzgerald et al., 2019b). These studies include both numerical and experimental  
57 investigations, and the majority of studies to date have focussed on bridges with deep  
58 foundations (piles). For a comprehensive overview of approaches based on changes in natural  
59 frequencies, interested readers are referred to Bao and Liu (2017).

60 Using numerical modelling, Prendergast et al. (2016a, 2016b) investigate how scour around  
61 the central pier of a two-span integral bridge influences the first natural frequency of the  
62 structure and study the ability to use changes in this frequency to detect scour. The influence  
63 of parameters such as vehicle speed and mass, road surface roughness and sensor ‘noise’, on  
64 the resulting lateral pier vibrations are studied to ascertain how robust the approach is for scour  
65 detection. They conclude that monitoring frequency changes shows potential to detect scour  
66 erosion. The approach is extended in Prendergast et al. (2017) to detecting the location of scour  
67 on a two-span integral bridge, i.e. which pier or abutment is scoured, by analysing multiple  
68 frequencies from the bridge with a focus on local element frequencies. Kong and Cai (2016)

69 numerically investigate the dynamic response of a continuous four-span bridge under wave  
70 loads and demonstrate that scour has a significant effect on the lower frequencies of a bridge  
71 pile. Furthermore, it is shown how scour affects the complete bridge-vehicle-wave system,  
72 meaning that the response of the bridge deck or even a passing vehicle can also be used to  
73 monitor scour. Ju (2013) studies how the natural frequency of a bridge varied due to scour  
74 using numerical modelling. It is shown how water-added mass surrounding the foundations  
75 influences the frequency values and it is concluded that its presence lowers the frequency.  
76 However, accounting for water-added mass is difficult and it is recommended that it can be  
77 ignored in bridge frequency analyses. Chen et al. (2014) present a scour monitoring approach  
78 using velocity sensors and a finite-element model of a cable-stayed bridge. Combining sensor  
79 measurements with FE updating enables scour of the pier to be quantified. Klinga and Alipour  
80 (2015) perform numerical analyses on the performance of various bridge elements under  
81 extreme scour and conclude that scour reduces lateral stiffness and lowers the natural  
82 frequency. Xiong et al. (2018a) propose a scour indicator based on the bridge flexibility matrix,  
83 which is sensitive to scour-induced changes on the frequencies and mode shapes of the  
84 structure. Bao et al. (2017) perform numerical and experimental studies to investigate three  
85 particular issues with frequency-based scour detection, namely (i) the physical meaning of the  
86 predominant natural frequency (PNF), (ii) the optimal location for installed sensors, and (iii)  
87 the influence of scour hole shape. By comparing a modal PNF to one obtained from dynamic  
88 testing, separation of bridge (structural) frequencies and soil (or computational domain)  
89 frequencies is possible. In terms of optimal sensor location, they suggest locating sensors at a  
90 point near maximum modal amplitude. For the structure considered in their paper, this is the  
91 top of the pier (free end). Furthermore, they propose a new criterion to define scour depths in  
92 asymmetrical scour situations to ensure a smooth variation of PNF with scour.

93 Several authors have trialled other types of (non-frequency) vibration-based scour detection  
94 methods on both laboratory-scale and full-scale bridges. Foti and Sabia (2010) present a study  
95 on a full-scale five span bridge where one of the piers experienced historical scour issues. By  
96 monitoring the asymmetric dynamic behaviour of the pier (due to variations in upstream and  
97 downstream scour) using the covariance of accelerations measured by an array of sensors along  
98 the foundation, they conclude that scour presence is detectable (but the extent is not  
99 quantifiable). Briaud et al. (2011) undertook experimental testing on a scaled-model bridge and  
100 investigated the performance of a range of approaches at detecting scour. One particular  
101 approach was to analyse the root-mean-square of acceleration signals measured in various  
102 directions and to use this as an indicator of scour occurrence. The ratio of RMS values showed  
103 sensitivity to scour development (Prendergast and Gavin, 2014).

104 The use of mode shapes to detect scour is a relatively recent development. However, mode  
105 shapes have been used in other damage detection fields to detect general forms of structural  
106 damage (cracks etc.). Damage detection methods based on changes in mode shapes are an  
107 alternative to natural frequency-based approaches, and can be advantageous in detecting local  
108 damage, and are not as prone to issues such as changes in temperature (Sohn, 2006). Structural  
109 damage detection using mode shapes generally consists of either comparing two modes from  
110 different health states of the structure, extracting features of the mode shape (e.g. curvature)  
111 that are sensitive to damage, or applying signal processing techniques to mode shape data (Fan  
112 and Qiao, 2011). Two common methods to compare shapes are Modal Assurance Criterion  
113 (MAC) and Coordinate Modal Assurance Criterion (COMAC) (Allemang and Brown, 1982,  
114 Dos Santos et al., 2000). MAC is a measure of the correlation between two modes with a value  
115 of unity representing a perfect match and a value of zero representing no match between the  
116 two modes. Hence, a reduction in MAC value may indicate the presence of damage. Salawu  
117 and Williams (1995) test MAC on mode shapes obtained from a concrete bridge before and

118 after repair and find that the MAC values change significantly in comparison to the measured  
119 frequency changes. COMAC is a pointwise comparison of two mode shapes, with a low  
120 COMAC value indicating possible damage at that point. Frýba and Pirner (2001) use COMAC  
121 in the repair of a segmentally constructed pre-stressed concrete bridge and show that the  
122 COMAC analysis of a repaired segment was similar to that of an undamaged segment.

123 Pandey et al. (1991) show, using an analytical model, that the mode shape curvature (i.e. the  
124 second derivative of the mode shape) can detect damage in both a simply supported beam and  
125 a cantilever beam. Wahab and De Roeck (1999) use a mode shape curvature-based method on  
126 the Z24 bridge in Switzerland and develop an indicator based on the difference in curvatures  
127 before and after damage. Other authors have shown, however, that mode shape curvatures are  
128 poor for detecting smaller amounts of damage (Ratcliffe, 2000). More detailed reviews of other  
129 approaches using mode shapes are depicted in (Carden and Fanning, 2004, Fan and Qiao, 2011,  
130 Moughty and Casas, 2017, OBrien and Malekjafarian, 2016, Malekjafarian and OBrien, 2017,  
131 Kong et al., 2017).

132 Some previous studies have used mode-shape based approaches to detect and monitor scour  
133 erosion. Elsaid and Seracino (2014) investigate the influence of scour on a scaled model of a  
134 coastal bridge. Scour is modelled as an increase in the effective length of bridge piles extending  
135 from the deck. Mode shape curvature, flexibility-based deflection and flexibility-based  
136 curvature are assessed to ascertain their performance at scour monitoring. The study concludes  
137 that horizontally-displaced mode shapes show sensitivity to the modelled scour. Moreover, the  
138 change in the mode shape curvature, flexibility-based deflections and curvatures showed  
139 promise in identifying the existence, location and possibly the extent of scour. Xiong et al.  
140 (2018b) investigate four scour indicators for a scoured cable-stayed bridge, namely frequency  
141 change ratio, MAC, modal curvature and flexibility-based deflection. Flexibility-based  
142 deflection is recommended as the most practical way to detect scour. In a separate study, Xiong

143 et al. (2019) present a scour identification approach based on measuring the ambient vibration  
144 of the superstructure of a cable-stayed bridge. By analysing the change in the mode shapes at  
145 two different times, qualitative scour identification is possible. The authors furthered the  
146 procedure to enable quantitative scour identification using a companion FE model of the  
147 system, whose soil stiffness is updated to match the real system.

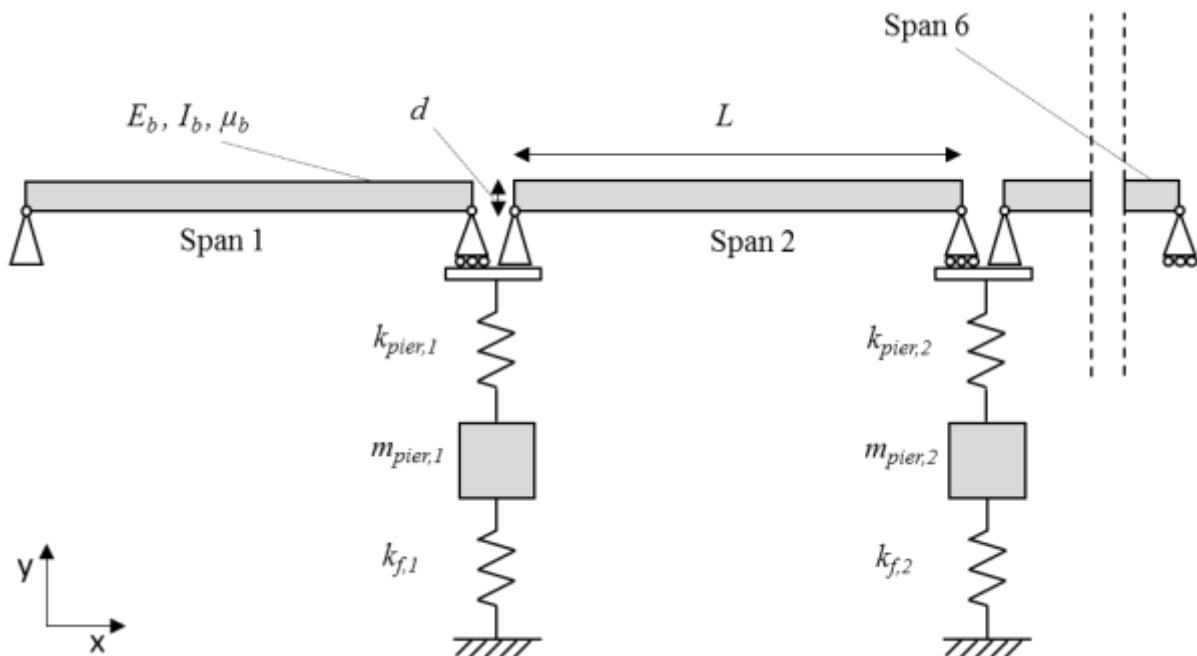
148 The majority of previous works on vibration-based scour monitoring have focussed on changes  
149 in natural frequencies to detect scour presence. Approaches using mode shapes have generally  
150 focussed on direct comparison of pre- and post-scour modes using MAC-type analyses or have  
151 used modal curvature and flexibility-based deflection. The majority of these studies have been  
152 applied to cable-stay bridges or bridges with piled foundations. The contribution of the present  
153 work relates to the use of information from the mode shape as identified from output-only  
154 modal identification to detect local reductions in stiffness resulting from scour-related stiffness  
155 losses. The approach developed is applicable to vertical stiffness loss experienced at shallow  
156 foundations, since a majority of previous works have focussed on identifying changes in lateral  
157 stiffness as would be expected at deeper foundations. Furthermore, the approach is  
158 demonstrated in this paper using scaled experimental testing. The first global mode shape of  
159 an experimentally scaled bridge with multiple spans is extracted using Frequency Domain  
160 Decomposition (FDD) (Brincker et al., 2001). Accelerations from the bridge midspans and  
161 piers are used as the input to the FDD algorithm, arising due to a model vehicle traversing the  
162 structure.

163 A novel scour indicator is proposed whereby the mode shape amplitude at one pier is compared  
164 to the mean of the mode shape amplitudes at the remaining piers in a process that creates a  
165 Mean-Normalised Mode Shape (MNMS). It is shown that at the scoured pier, the MNMS value  
166 increases due to a loss of stiffness as a result of scour. Moreover, the magnitude of the MNMS  
167 at a scoured pier increases with further decreases in stiffness. The approach is also capable of

168 detecting which pier is scoured by considering the nature of the changes in the MNMS. The  
169 MNMS approach is an improvement on using the mode shape of the system alone, as it is more  
170 sensitive to scour than changes in mode shape obtained from MAC analysis. Moreover, only  
171 one mode shape is required, namely the damaged mode shape, to derive the required  
172 information. This means that a reference (undamaged) mode shape is not required, as would  
173 be the case when comparing modes using MAC. The method only requires sensors located at  
174 piers so does not suffer from the requirement of many sensors, as would be needed for accurate  
175 estimates of modal curvature, for example. The method may be suited to output-only scour  
176 identification for multi-span bridges founded on shallow pad foundations, which typically have  
177 not received much attention in the literature.

## 178 Scour monitoring approach based on pier mode shape values

### 179 Numerical Model



180

181

Fig. 1: Numerical model schematic

182 A numerical model is used to introduce the scour detection procedure and a schematic of this  
183 is shown in Fig. 1. It represents a bridge with pinned connections (internal hinges) between  
184 each of six spans. Each pier is assumed to rest on a shallow pad foundation with underlying  
185 soil stiffness. Each span is modelled as a simply supported Euler-Bernoulli beam, the mass and  
186 stiffness matrices for which are available in (Kwon and Bang, 2000). The beginning and end  
187 of the bridge are assumed to rest on undeformable abutments, which are modelled as pinned,  
188 and roller supports, respectively. Hence, there are five internal piers. Twenty 1 m long beam  
189 elements are used for each span in the finite-element model. The beams are connected using  
190 nodal hinges with a supporting pier at each connection, modelled as a single degree of freedom  
191 (DOF) sprung-mass in the vertical direction.

192 Each pier is supported by a spring,  $k_f$ , which represents the vertical stiffness provided by a  
193 shallow pad foundation with notional length,  $L$  and width,  $B$  dimensions of 4 m and 2 m  
194 respectively. Using these pad dimensions, the stiffness of the spring is calculated using the  
195 approach in FEMA (2000), see Eq. (1),

$$k_f = \frac{GB}{1-\nu} \left[ 1.55 \left( \frac{L}{B} \right)^{0.75} + 0.8 \right] \quad (1)$$

197 where  $G$  is the operational shear modulus of the soil ( $\text{kN m}^{-2}$ ) and  $\nu$  is the small-strain Poisson  
198 ratio. An elastic modulus,  $E = (2G(1+\nu))$ , corresponding to a medium dense sand (Prendergast  
199 and Gavin, 2016) is assumed for the unscoured stiffness. Note, the expression in Eq.(1) is semi-  
200 empirical and there exists several formulations that take this approximate form (Pais and  
201 Kausel, 1988, Mylonakis et al., 2006). Table 1 lists the main geometrical and material  
202 properties of the bridge. The second moment of area is calculated by assuming a 4 m wide  
203 single-track railway bridge with a rectangular cross-section and the mass and stiffness of the  
204 pier is calculated by assuming pier dimensions of 7 m (in y-direction), 1 m (in x-direction) and

205 2.5 m (into page) with a modulus of elasticity and density of  $35 \times 10^6 \text{ kN m}^{-2}$  and  $2400 \text{ kg m}^{-3}$   
 206 respectively.

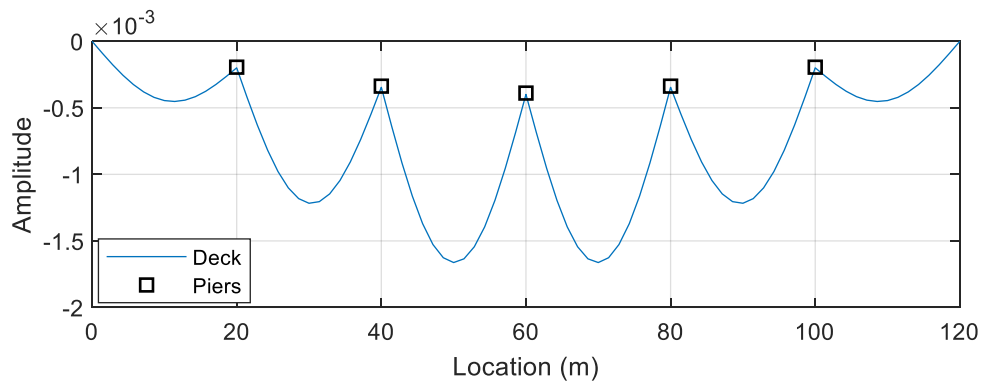
207 Table 1: Properties of bridge used to introduce the scour identification approach

Property	Symbol	Unit	Value
Span length	$L$	m	20
Beam depth	$d$	m	1
Beam second moment of area	$I_b$	$\text{m}^4$	0.33
Beam modulus of elasticity	$E_b$	$\text{kN m}^{-2}$	$35 \times 10^6$
Beam mass per unit length	$\mu_b$	$\text{kg m}^{-1}$	$9.60 \times 10^3$
Pier mass	$m_{pier}$	kg	$42 \times 10^3$
Pier stiffness	$k_{pier}$	$\text{kN m}^{-1}$	$12.50 \times 10^6$
Vertical stiffness provided by shallow pad foundation	$k_f$	$\text{kN m}^{-1}$	$344.12 \times 10^3$

208

209 In this work, scour is modelled as a reduction in stiffness of a given vertical foundation spring.  
 210 It is worth noting that in the real case a loss of rotational stiffness could occur as a result of  
 211 scour which would result in rocking effects on the pad. This type of situation could arise in the  
 212 case of asymmetric scour affecting the foundation (Foti and Sabia, 2010). However, the present  
 213 study specifically focuses on vertical stiffness loss only (Eq. 1). The basis for scour-related  
 214 stiffness loss lies in the stress and strain dependency of soil stiffness, as discussed herein. The  
 215 shear modulus of soil ( $G$ ) typically increases nonlinearly with mean effective stress. The  
 216 magnitude of this shear modulus at a given depth is a function of the amount of overburden  
 217 pressure at that location. Scour leads to a local reduction in soil elevation relative to a  
 218 foundation, which implies the overburden pressure reduces in the vicinity of scoured  
 219 foundations (Zhang et al., 2017). It can therefore be assumed that scour occurrence would  
 220 change the operational shear modulus at formation level, although by a small amount. In  
 221 extreme cases, however, scour can undermine a shallow pad (Scozzese et al., 2019). When this  
 222 occurs, the contact area between the remaining soil beneath the shallow foundation and the pad  
 223 is reduced, leading to increased stress on the remaining soil from the applied loads. This

224 increased stress subsequently increases the strain in the soil, due to the typically nonlinear  
225 stress-strain relationship of soil. Additionally, the shear modulus of soil is strain-dependant,  
226 and typically reduces with strain (Oztoprak and Bolton, 2013, Hardin and Drnevich, 1972). In  
227 this paper, both the aforementioned mechanisms are assumed to occur leading to a reduction  
228 in the vertical stiffness of a foundation under scour. For the geometries considered in the  
229 present study, a 30% example loss in stiffness would be expected if the foundation was  
230 undermined by scour reducing the soil-foundation contact area from  $8\text{m}^2$  ( $4\text{m} \times 2\text{m}$ ) to  $5.1\text{m}^2$   
231 ( $3\text{m} \times 1.7\text{m}$ ), with a corresponding reduction in soil shear modulus,  $G$  equating to 10%  
232 reduction from the small-strain value  $G_0$  (Oztoprak and Bolton, 2013).



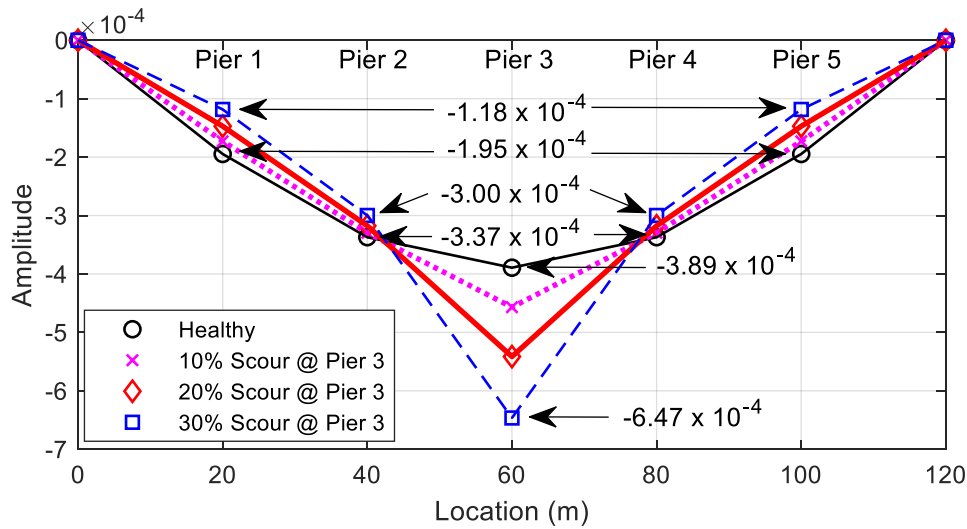
233

Fig. 2: First mode shape of system for healthy case - 3.70 Hz frequency

234

235 Fig. 2 shows the first global mode shape of the bridge corresponding to the first natural  
236 frequency of the system when there is no scour. The mode shape is derived from the system  
237 mass and stiffness matrices by solving the Eigenproblem (Clough and Penzien, 1993). As is  
238 evident, each of the bridge spans exhibit a bending shape with each of the piers exhibiting  
239 motion in the same direction for this mode. The central pier has the highest maximum mode  
240 shape amplitude relative to the remaining piers. The first mode shape of the bridge will be used  
241 to develop a scour monitoring approach by investigating the sensitivity of this mode to scour  
242 at various locations.

243 **Mean-Normalised Mode Shape (MNMS) to detect Scour**



244

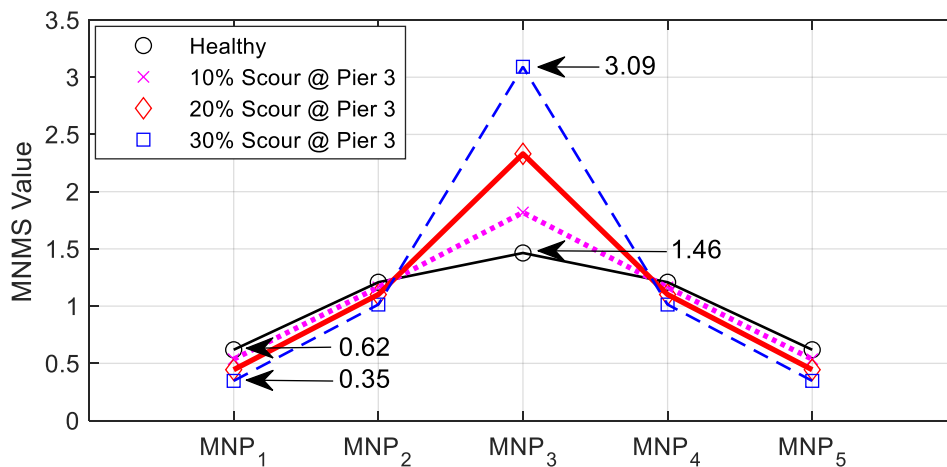
245 Fig. 3: First mode shape amplitude at pier locations of bridge system due to varying levels of stiffness loss as a  
 246 result of scour at Pier 3 (60 m point).

247 Fig. 3 shows how the stiffness loss due to scour affects the first mode shape of the system for  
 248 scour at the central pier of the bridge. In this plot, the percentage scour refers to percentage  
 249 stiffness loss as a result of scour, and is defined as the reduction in vertical foundation stiffness  
 250 with respect to the stiffness of a foundation with zero scour. Only the mode shape values at the  
 251 pier locations are shown here and the spans are simplified as straight lines. For each scenario,  
 252 the modes are normalised with respect to the system mass matrix so that they can be  
 253 quantitatively compared. In this work, a scour indicator based on the first mode shape  
 254 amplitudes at the locations of the piers is proposed. The first mode shape is used to develop the  
 255 scour indicator because for this mode, all of the piers exhibit movement in the same direction  
 256 enabling a ratio-type indicator to be created. Fig. 3 shows that the largest change in the mode  
 257 shape amplitude occurs at the scoured pier. It is of note that the mode shape amplitude is  
 258 affected at unscoured piers also. At the scoured pier the absolute value of the modal amplitude  
 259 increases with an increase in scour (reduced stiffness). At unscoured piers, the opposite effect  
 260 is observed whereby the absolute value of the amplitude decreases with an increase in scour. It  
 261 should be noted that the changes at the scoured pier are much greater than those at the

262 unscoured piers. Based on this premise, a scour indicator referred to as the Mean Normalised  
 263 Mode Shape (MNMS) is proposed to compare the mode shape value of a given pier with those  
 264 at the other piers. The mean value of the modal amplitudes of the remaining piers is used as  
 265 the metric to compare each pier mode shape value. In mathematical form, the MNMS at any  
 266 pier is represented as Eq. (2).

$$267 \quad \{MNMS\}_x = \frac{\{MS\}_x}{\frac{1}{n-1} \sum_{\substack{k=1 \\ k \neq x}}^n \{MS\}_k} \quad (2)$$

268 where  $n$  is the total number of piers, which in this case is equal to five,  $x$  is the pier number  
 269 such that  $x \in \{1:n\}$ ,  $MS$  is a vector of pier mode shape amplitudes and the summation term  
 270 represents the sum of the pier mode shape amplitudes excluding Pier  $x$ .



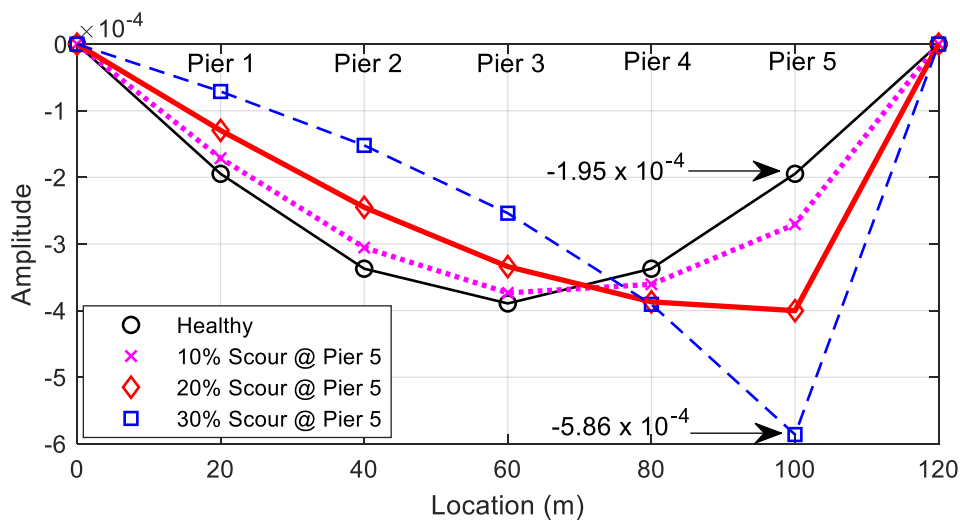
271

272 Fig. 4: MNMS values for each pier for varying levels of scour at Pier 3

273 Fig. 4 shows how the MNMS at each pier is affected by the stiffness loss due to scour at Pier  
 274 3. At the scoured pier (Pier 3), the MNMS increases with an increase in scour severity from  
 275 1.46 when there is no scour affecting the bridge to 3.09 when scour corresponding to a 30%  
 276 decrease in Pier 3 foundation stiffness affects the structure. At other (unscoured) piers, the

277 MNMS values decrease with an increase in scour severity at Pier 3. For example, the MNMS  
 278 value at Pier 1 decreases from 0.62 to 0.35 where there is 30% scour at Pier 3.

279 It is clear that the MNMS pattern (Fig. 4) has a strong resemblance to the mode shape values  
 280 themselves (Fig. 3). The main advantage of using the MNMS over direct mode shape  
 281 comparison lies with the fact that for mode shapes, normalisation is required to facilitate  
 282 comparison. The mode shapes derived from an output-only modal method like FDD are not  
 283 mass-normalised as the input forces are unknown (Khatibi et al., 2012). This means that the  
 284 magnitude of the mode shape values depends on the amplitude of the input forces. For example,  
 285 a passage of a heavy vehicle may generate signals with higher modal amplitudes than a lighter  
 286 vehicle. The normalisation process could affect the observed changes due to scour. A common  
 287 practice for depicting operational mode shapes is to normalise them with respect to their  
 288 maximum value (Khatibi et al., 2012). However, normalising the mode shapes in this way  
 289 could lead to a situation where the modes exhibit no change at the location of the scoured pier  
 290 – which would be the case in Fig. 3. The metric defined in Eq. (2) avails of the relative changes  
 291 in the mode at various points, therefore it is insensitive to changes in modal magnitude resulting  
 292 from the passage of different vehicles.



293  
 294 Fig. 5: First mode shape amplitude at pier locations of bridge system due to varying levels of stiffness loss as a  
 295 result of scour at Pier 5 (100 m point).

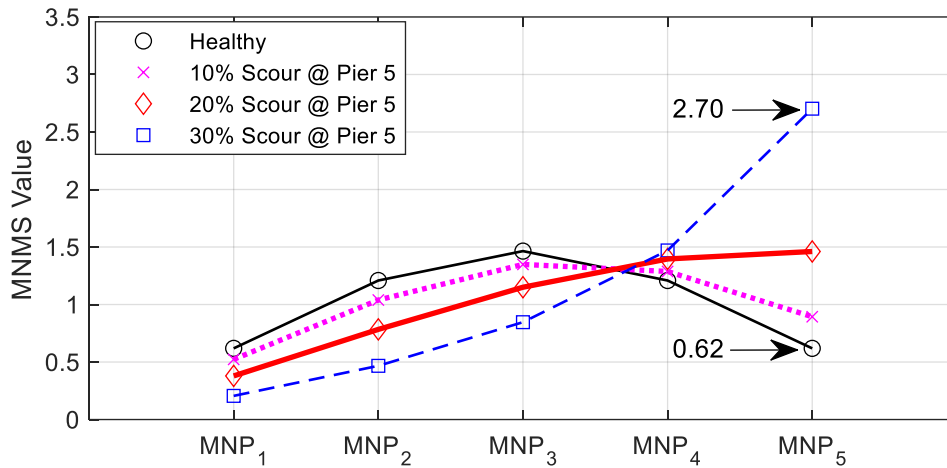


Fig. 6: MNMS values for each pier for varying levels of scour at Pier 5

296

297

298

299

300

301

302

303

304

305

306

307

308

Fig. 5 shows how increasing stiffness loss at Pier 5 influences the mode shape amplitudes at each pier. Fig. 6 shows the corresponding MNMS values at each pier. The MNMS values defined in Eq. (2) experience a greater percentage change at the scoured pier than the raw mode shape values at this location (335% as opposed to 200% for the 30% scour case). Note also that the mode shapes in this case are mass-normalised mode shapes directly from Eigen-analyses. In the real case, they would have to be computed from time domain data, making them less reliable. Fig. 6 exhibits a broadly similar trend to that of Fig. 4 in that at the scoured pier, the MNMS value increases while at the unscoured piers it decreases. However, in this case, Pier 4 which is closest to the scoured pier also exhibits an increase in MNMS value. The mode shape itself also reflects this (see Fig. 5) as both Piers 4 and 5 show an increase in absolute mode shape value due to scour at Pier 5.

### 309 **Frequency Domain Decomposition (FDD)**

310

311

312

313

314

It is not possible to extract the mode shapes using an eigenvalue analysis on a real structure. Instead, it is necessary to derive modal information by analysing time-domain signals measured from a target structure. In this work, Frequency Domain Decomposition (FDD) (Brincker et al., 2001) is used as a means to extract mode shapes from acceleration measurements. FDD is an output-only modal identification method, i.e. it enables estimation of the system dynamic

315 parameters without prior knowledge of the input excitation. The approach is suitable for a  
316 scenario where a bridge is excited by unknown vehicle properties.

317 FDD begins with the estimation of the power spectral density (PSD) matrix,  $\hat{G}(j\omega)$ , from the  
318 various responses at discrete frequencies for  $\omega=\omega_i$ . Next,  $\hat{G}(j\omega)$  is decomposed at each  
319 frequency by applying Singular Value Decomposition (SVD) (Brincker et al., 2001) to obtain  
320 Eq. (3).

$$321 \quad \hat{G}(j\omega_i) = U_i S_i U_i^H \quad (3)$$

322 where  $U_i$  is a unitary matrix of singular vectors,  $S_i$  is a diagonal matrix holding the singular  
323 values and  $H$  denotes the complex conjugate of the matrix. Using the singular values obtained  
324 at each frequency, an SVD diagram can then be plotted. From this plot, the natural frequencies  
325 of the structure can be obtained from the dominant peaks and the corresponding singular  
326 vectors are the mode shapes.

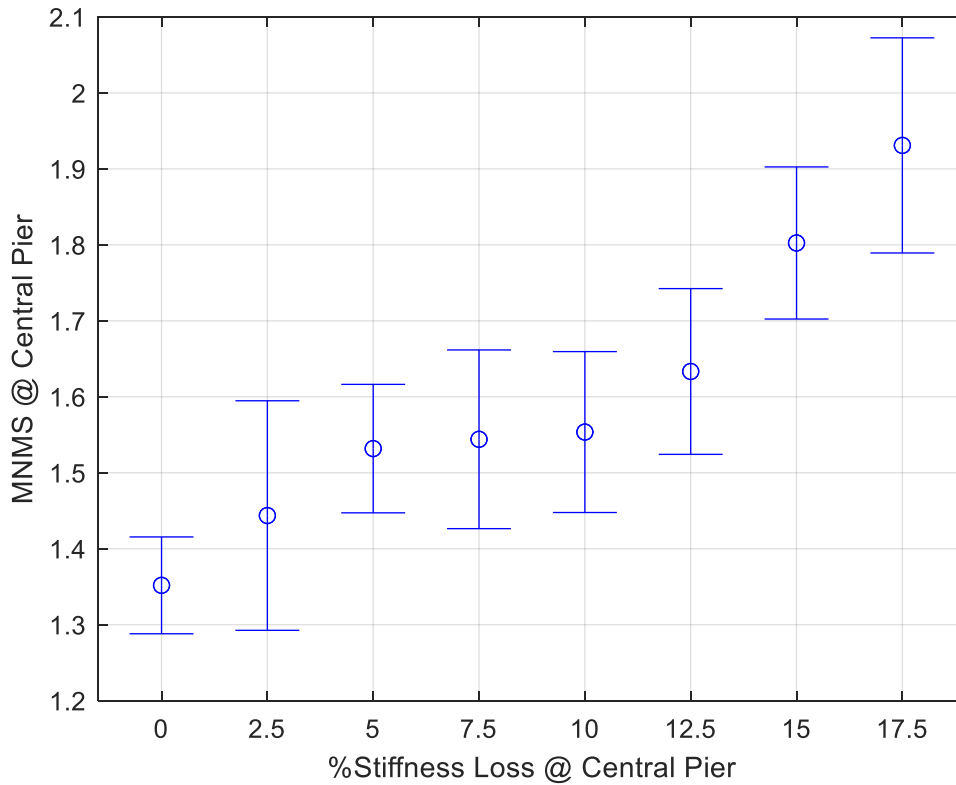
### 327 **Minimum stiffness loss that can be detected by the MNMS approach under** 328 **noisy conditions**

329 It is of interest to assess the minimum stiffness loss that can be detected by the approach  
330 postulated in this paper. To investigate this, a time-domain analysis is conducted whereby the  
331 external excitation is by means of a simulated quarter car crossing the bridge model described  
332 previously. A quarter car (with two degrees of freedom and crossing speed of 80 km/h) is  
333 coupled with the bridge model to form a vehicle-bridge interaction (VBI) model (Keenahan et  
334 al., 2013, OBrien et al., 2017) and properties of the quarter car are taken from the literature  
335 (Fitzgerald et al., 2019b). Forced vibration data and 5s of free vibration pier acceleration data  
336 extracted from the VBI model is inputted to the FDD algorithm from which the mode shapes  
337 are extracted. Before they are inputted into the FDD algorithm, noise is added to the clean

338 acceleration signals from the model to generate more realistic accelerations. Random noise is  
339 added to the acceleration signals using Eq. (4):

$$340 \quad \{a\} = \{a_{calc}\} + E_p \{N_{noise}\} \{a_{max}\} \quad (4)$$

341 where  $a$  is the noisy acceleration signal,  $E_p$  is the level of noise,  $N_{noise}$  is a normally distributed  
342 vector with a standard deviation equal to one,  $a_{calc}$  is the clean acceleration signal outputted  
343 from the VBI model and  $a_{max}$  is the maximum value of the signal. The level of noise is chosen  
344 to be 5%, which is consistent with values used in the literature (Zhu and Law, 2002,  
345 Malekjafarian and OBrien, 2014). Keeping the same excitation source, the mode shape  
346 extraction process is repeated 10 times, each for a healthy bridge case, and seven scour  
347 scenarios ranging from a 2.5% to 17.5% stiffness loss at the central bridge pier. The MNMS is  
348 calculated for each run in every scenario, enabling mean and standard deviations of MNMS  
349 values to be obtained for each case. Fig. 7 shows an error bar plot (mean +/- one standard  
350 deviation) for the MNMS value of the central pier. It can be seen that there are overlaps in the  
351 error bars for the lower stiffness loss cases and the healthy case (0% stiffness loss). At around  
352 7.5% stiffness loss, there is a clear distinction relative to the error bars of the healthy case.  
353 However, the error bars for stiffness losses between 2.5% and 12.5% show an overlap with one  
354 another. This suggests that a more realistic estimation for the minimum stiffness loss that can  
355 be detected would be greater than 10%. Here, for differences of 12.5%, there are no overlaps  
356 between the error bars.



357

358

Fig. 7: Minimum scour detectable considering natural variation due to noise of MNMS

359

## Experimental Model

360

The previous sections introduced the concept of MNMS and demonstrated it via numerical

361

modelling. In this section, a scaled model of a bridge with multiple simply supported spans has

362

been developed to experimentally validate the MNMS concept. The tests were conducted in a

363

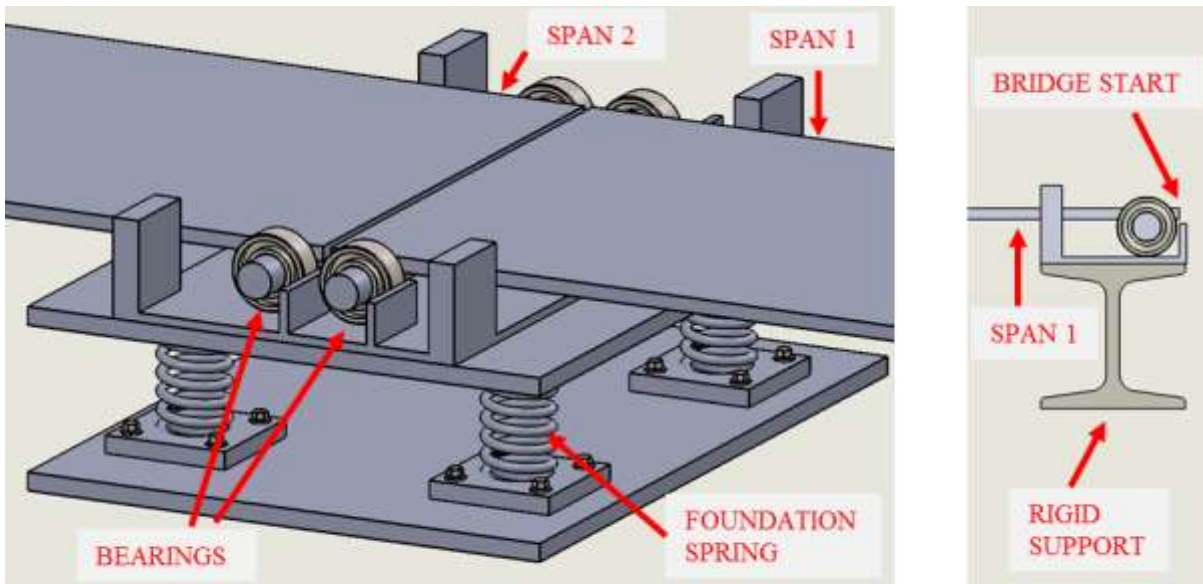
laboratory at Kyoto University in Japan.

364 **Bridge**



(a)

365



(b)

(c)

366

367 Fig. 8: Experimentally scaled multi-span bridge (a) full bridge (b) pier supported on four springs (in this case  
368 Pier 1) (c) rigid support at bridge extremes

369 The model bridge consists of four spans supported on three piers - see Fig. 8(a). The bridge  
370 was traversed by a scaled model vehicle to generate the external excitation. Each pier was  
371 founded on four springs of equal stiffness, to provide vertical stability, and bearings were used  
372 to create pin and roller supports (Fig. 8(b)). The start and end of the bridge rest on rigid supports  
373 and do not deflect (Fig. 8(c)). Table 2 provides the properties of the beam used for each bridge  
374 span.

375

Table 2: Span details

Property	Unit	Value
Span length	mm	1300
Width	mm	300
Beam depth	mm	8.07
Second moment of area (rectangular cross section)	m <sup>4</sup>	1.31 × 10 <sup>-8</sup>
Modulus of elasticity	N m <sup>-2</sup>	2.05 × 10 <sup>11</sup>
Density	kg m <sup>-3</sup>	7850

376

377 The stiffness of the foundation springs was determined from load-displacement testing and  
 378 benchmarked against geotechnical analyses assuming small-strain linear behaviour, which is  
 379 appropriate for bridges traversed by moving vehicles. Spring values were defined for the scaled  
 380 model and a scaling criterion was applied to check compliance at full-scale dimensions, as  
 381 described herein. The stiffness of each spring used in the experiment (for the healthy bridge  
 382 scenario) is 49 N mm<sup>-1</sup>. As four springs were used in parallel beneath each pier, the  
 383 experimental equivalent stiffness under each support,  $k_{f,EXP}$ , was 196 N mm<sup>-1</sup>. In order to  
 384 achieve compliance with an equivalent full-scale model, a scaling criterion is defined as the  
 385 ratio of (i) the midspan deflection of a simply supported beam with a unit static load applied  
 386 directly at midspan, and (ii) the deflection of the support spring when a unit static load is  
 387 applied directly over a pier. In the numerical model employed to introduce the procedure in the  
 388 previous section, the stiffness of the pier ( $k_{pier}$ ) is greater than the foundation stiffness ( $k_f$ ) by a  
 389 factor of 36. Therefore, in this criterion the equivalent stiffness of the two in series is governed  
 390 by the stiffness provided by the shallow pad foundation.

391 In mathematical form, the midspan deflection of a simply supported beam due to a static unit  
 392 load at the centre is shown in Eq. (5)

393

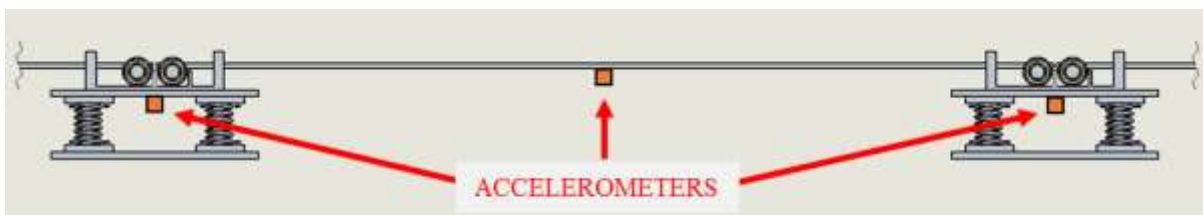
$$d_{mid} = \frac{L^3}{48EI} \quad (5)$$

394 where  $L$  is the beam span length,  $E$  is the Young's Modulus and  $I$  is the beam second moment  
 395 of area. The deflection at a pier,  $d_{pier}$ , due to a unit static load immediately overhead, is simply  
 396 the reciprocal of the stiffness provided by the shallow pad foundation (i.e.  $1/k_f$ ). By maintaining  
 397 the ratio of  $d_{mid}$  to  $d_{pier}$  between a full-scale numerical model and the scaled experiment, the  
 398 experimental foundation stiffness can be represented as Eq. (6)

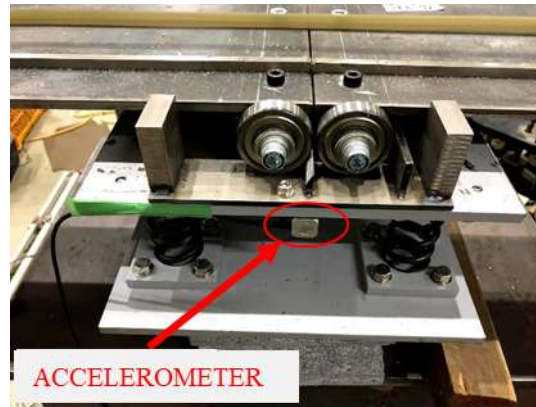
$$399 \quad k_{f,EXP} = k_{f,NUM} \left( \frac{L_{NUM}^3 E_{EXP} I_{EXP}}{L_{EXP}^3 E_{NUM} I_{NUM}} \right) \quad (6)$$

400 where subscripts  $EXP$  and  $NUM$  denote the experimental and numerical full scaled model  
 401 respectively.

402 Using the scaling criterion defined in Eq. (6) and taking values of  $L$ ,  $E$  and  $I$  from Tables 1 and  
 403 2, the stiffness provided by an equivalent shallow pad foundation in a full-scale case,  $k_{f,NUM}$ , is  
 404 calculated to be  $234 \times 10^3 \text{ kN m}^{-1}$ . In order to check the validity of this assumption, a  
 405 benchmark geotechnical case is considered. Using the approach in Fitzgerald et al. (2019b) and  
 406 FEMA (2000), and taking appropriate values for sand shear modulus from Prendergast and  
 407 Gavin (2016), the stiffness provided by a shallow pad foundation of length, 4 m and width, 2  
 408 m is  $172 \times 10^3 \text{ kN m}^{-1}$  for a loose sand and  $344 \times 10^3 \text{ kN m}^{-1}$  for a medium dense sand. The  
 409 scaled experimental spring stiffness used in the present study lies within this range and can  
 410 therefore be understood to represent a loose to medium dense uniform sand deposit. The mass  
 411 of each pier,  $m_{pier}$ , was 12.56 kg, obtained from measuring the approximate volume of steel  
 412 directly above the four springs.



413

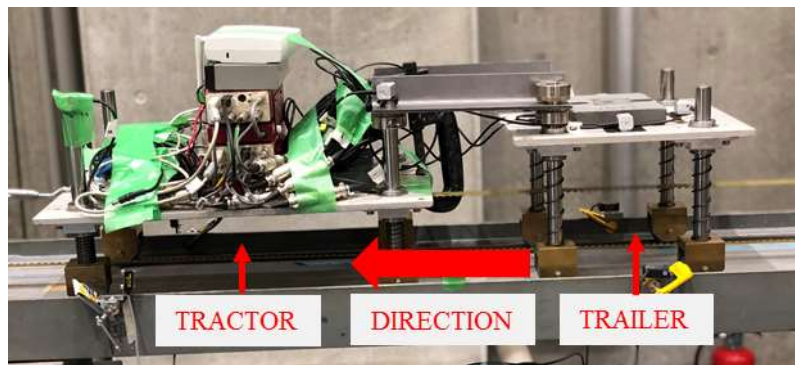


(b)

414

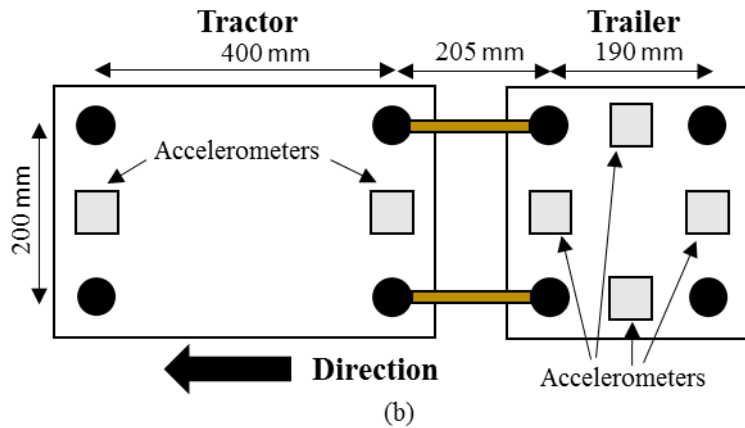
415 Fig. 9: Accelerometer locations (a) schematic of positions on midspan and pier (b) picture of one pier  
416 Accelerometers were installed on each of the piers and at the midspans (Fig. 9). Seven bridge  
417 acceleration measurements were recorded ( $3 \times$  Piers and  $4 \times$  Midspans). Optical sensors were  
418 also installed at the beginning and end of the bridge, enabling the timing of when each vehicle  
419 axle arrived and departed the bridge be obtained. To model the reduction in stiffness due to  
420 scour at a pier, the springs under the pier (Figs. 8(b), 9(b)) were replaced with four springs of  
421 a lower stiffness value for a given scour case. Two scour cases were considered, Case I where  
422 parallel springs, each of stiffness  $37 \text{ N mm}^{-1}$ , were used and Case II where parallel springs with  
423 stiffness of  $27 \text{ N mm}^{-1}$  were used. These cases equated to 24.5% and 44.9% stiffness reductions  
424 from the healthy case where each parallel spring had a stiffness of  $49 \text{ N mm}^{-1}$ .

## 425 Vehicle



(a)

426



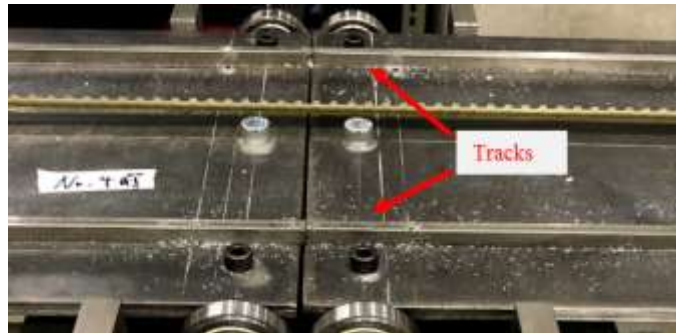
427

428 Fig. 10: (a) Experimental vehicle consisting of a tractor and trailer which are connected (b) Dimensions in plan  
429 view of the vehicle

430 The vehicle used in the experiments is shown in Fig. 10(a). It consisted of a two-axle tractor,  
431 connected to a two-axle trailer. Both the tractor and trailer consisted of sprung steel plates. The  
432 front tractor axle had two springs of stiffness  $1533 \text{ N m}^{-1}$  and the rear axle had two springs of  
433 stiffness  $1753 \text{ N m}^{-1}$ . The trailer had four equal axle suspension springs of stiffness  $8464 \text{ N m}^{-1}$ .  
434 The tractor and trailer had axle spacings of 400 mm and 190 mm respectively and the spacing  
435 between the rear tractor axle and front trailer axle was 205 mm (Fig. 10(b)).

436 The vehicle speed was kept constant by an electronic controller as it traversed the bridge.  
437 Traversing speeds of 1.14 m/s and 1.26 m/s were used in this experiment. Two different tractor  
438 masses, 24.3 kg and 26.3 kg were investigated to study potential sensitivity issues. The sprung  
439 mass (i.e. the mass supported by springs) of the tractor for these two weights was 20.7 kg and  
440 22.7 kg respectively. The trailer mass was 13.7 kg (of which 10.1 kg was sprung). The vehicle  
441 was maintained on the bridge by two steel tracks, see Fig. 11. Accelerometers were installed  
442 on the tractor and trailer in the locations shown in Fig. 10(b) which allows the vehicle  
443 frequencies to be calculated. The tractor had bounce and pitch frequencies of 3.1 Hz and 4.7  
444 Hz respectively (for the 20.7 kg case) and the trailer had bounce and pitch frequencies of 6.6  
445 Hz and 3.5 Hz respectively. These were obtained using free vibration vehicle acceleration  
446 measurements (after the vehicle has come to a halt) which were subsequently analysed using

447 Frequency Domain Decomposition (FDD) (Brincker et al., 2001), enabling the pitch and  
448 bounce modes be distinguished.



449

Fig. 11: Vehicle Tracks

450

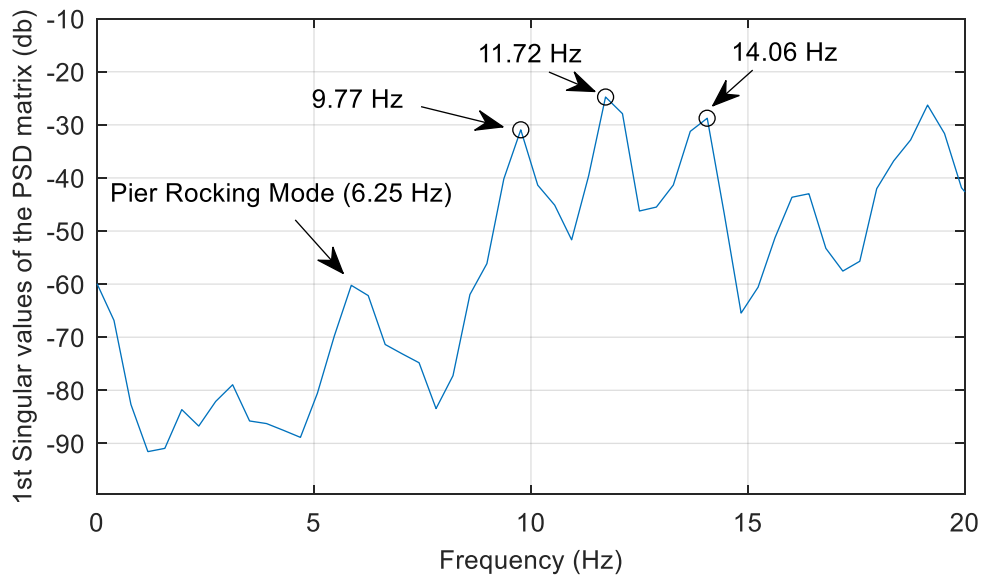
## 451 **Experimental Results**

452 The concept of using relative pier mode shape amplitudes is introduced in a previous section  
453 using theoretical mode shapes extracted from Eigen-analyses (Clough and Penzien, 1993) and  
454 a brief numerical demonstration. In this section, the procedure is applied to the acceleration  
455 signals generated at various points on a scaled bridge structure (see previous section) to  
456 ascertain how successful the approach is when the modal information is extracted directly from  
457 time signals incorporating natural experimental error.

## 458 **Procedure**

459 In the experimental tests, the model vehicle traversed the bridge at a specified velocity resulting  
460 in four acceleration measurements from the midspans and three from the piers. The resulting  
461 accelerations contain components relating to both the vehicle-induced vibrations and the  
462 subsequent free vibration. The time-domain signals are analysed using FDD to identify the  
463 mode shapes. Two vehicle speeds and tractor masses are investigated to ascertain how  
464 experimental variation influences the results. The FDD processing is undertaken in the  
465 MATLAB programming environment.

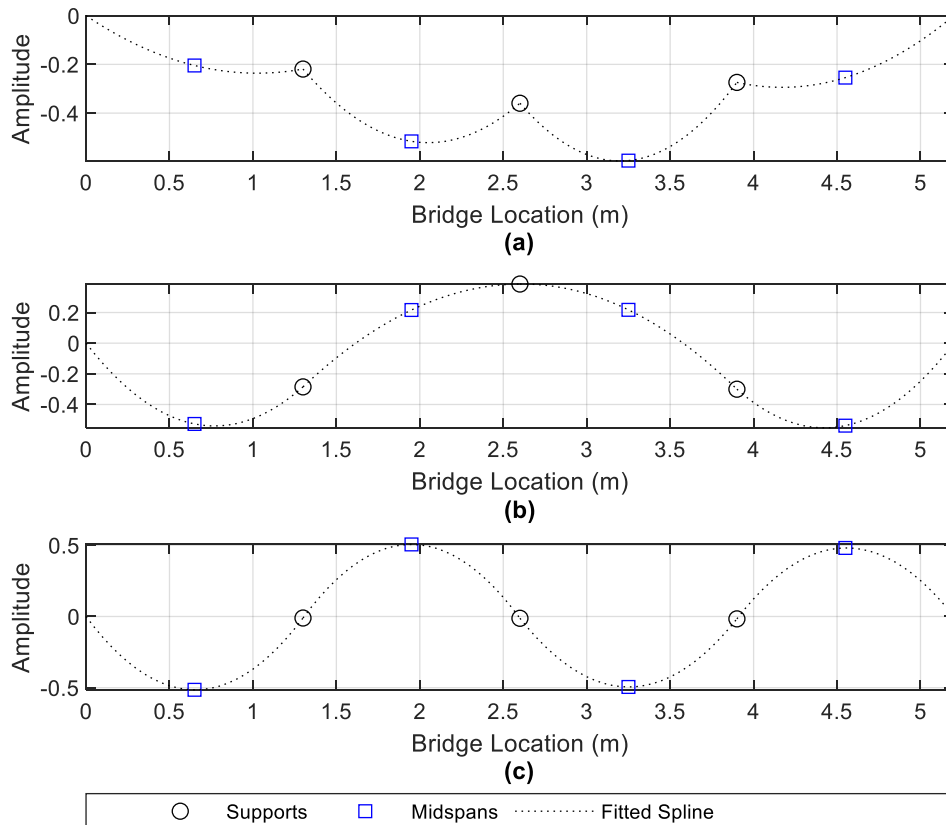
466 **Extraction of mode shapes for healthy case**



467

468 Fig. 12: Experimental FDD frequency picking from singular values of the spectral density matrix for vehicle  
469 crossing at speed of 1.26 m/s (with tractor mass of 22.7 kg)

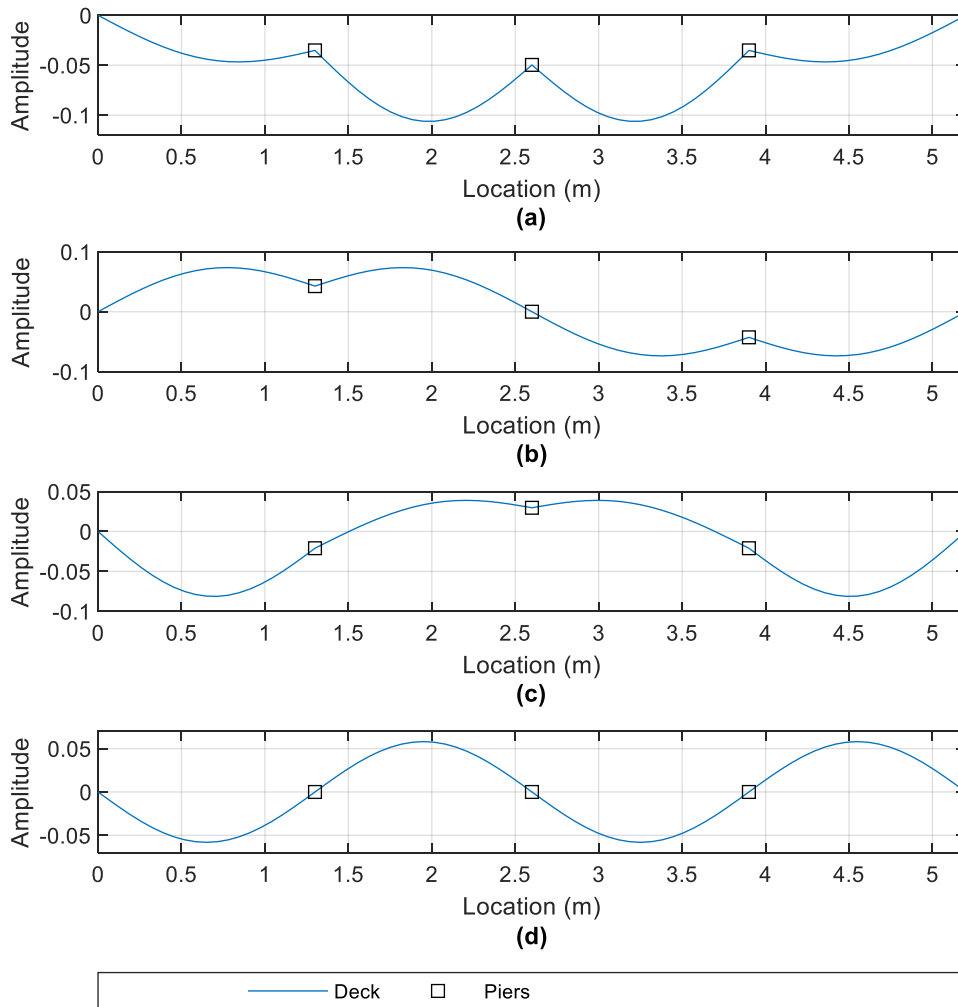
470 Fig. 12 shows the 1<sup>st</sup> singular values of the Power Spectral Density (PSD) matrix obtained by  
471 applying FDD to the seven acceleration signals resulting from the vehicle (with tractor mass  
472 of 22.7 kg) traversing the bridge at 1.26 m/s. As is evident, many peaks appear on the plot,  
473 each corresponding to a different mode of vibration. To demonstrate the process of deriving  
474 the mode shapes, three peaks are identified herein at 9.77 Hz, 11.72 Hz and 14.06 Hz. There is  
475 also a smaller peak visible at 6.25 Hz, which correlates to a pier rocking mode. Fig. 13 shows  
476 the extracted mode shapes corresponding to the three frequency peaks selected in Fig. 12. For  
477 ease of visualisation, a spline curve is fitted to the extracted points.



478

479 Fig. 13: Mode shapes derived from experimental accelerations - (a) 9.77 Hz mode, (b) 11.72 Hz mode, (c) 14.06  
480 Hz mode

481 Fig. 13(a) shows the first mode of the structure, at a frequency of 9.77 Hz. This mode shape  
482 resembles that of the numerical model of the full-scale structure shown in Fig. 2 in that all the  
483 piers are moving in the same direction. This is the ‘first’ mode shape and is the primary focus  
484 of the present work to detect a loss of stiffness due to scour. The 11.72 Hz mode (Fig. 13(b))  
485 differs from the 9.77 Hz mode in that Pier 2 (the centre pier) is moving in a different direction  
486 to Piers 1 and 3. Finally, in the 14.06 Hz mode (Fig. 13(c)), the piers exhibit negligible  
487 movement in comparison to the midspans. Due to this, the 9.77 Hz and 11.72 Hz modes would  
488 have an expected change due to scour but the 14.06 Hz mode would not (as the piers have  
489 insignificant modal amplitudes in this mode).



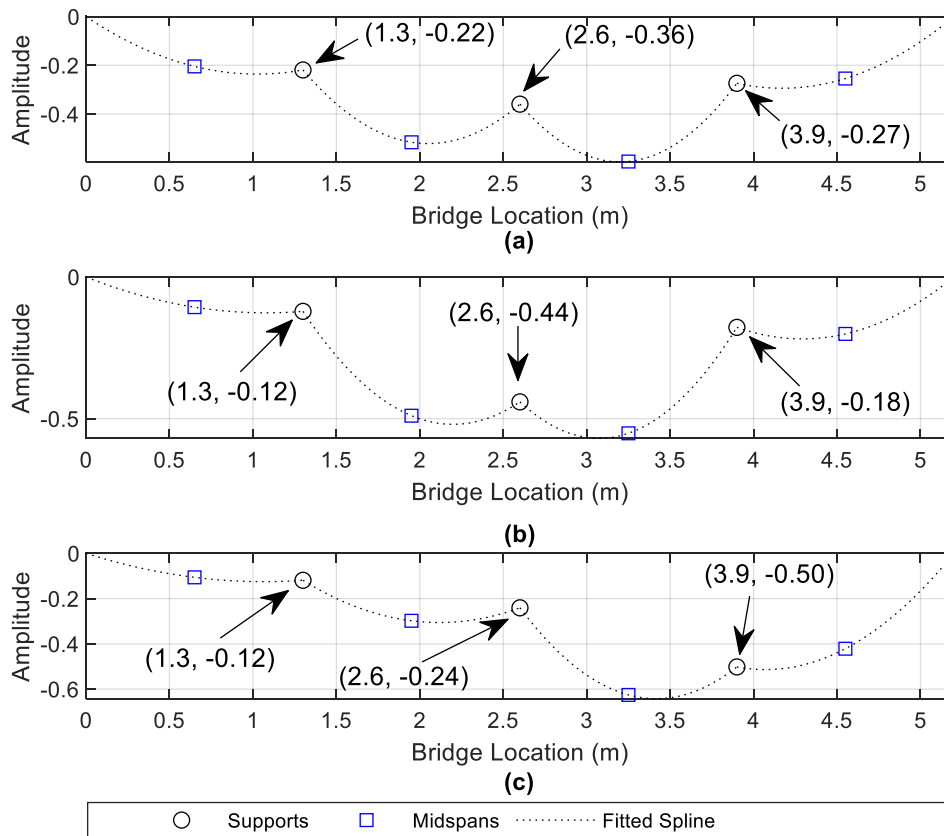
490

491 Fig. 14: First four mode shapes of system from numerical model - (a) 9.66 Hz mode, (b) 10.55 Hz mode, (c)  
 492 12.09 Hz mode, (d) 13.85 Hz mode

493 A numerical model of the scaled experimental arrangement is developed using the approach  
 494 described previously and using the experimental parameters in Table 2. Fig. 14 shows the mode  
 495 shapes of the first four frequencies derived from the numerical model by solving the  
 496 Eigenproblem of the system matrices (Clough and Penzien, 1993). It is worth noting that the  
 497 pier stiffness,  $k_{pier}$ , in the model is assumed to be infinite compared to the foundation stiffness,  
 498  $k_f$ . Here, the value of  $k_{pier}$  is selected by multiplying  $k_f$  by  $10^4$  (i.e. an arbitrary large number).  
 499 The steel tracks are also included in the numerical model so the beam second moment of area  
 500 and cross-sectional area are altered to account for this. With the tracks included, these  
 501 properties are  $21.67 \times 10^3 \text{ mm}^4$  and  $2549 \text{ mm}^2$  respectively.

502 A comparison of the experimental mode shapes (Fig. 13) derived from the time-domain  
503 acceleration signals and the numerically calculated ones (with the experimental model  
504 parameters - Fig. 14) shows clear similarities. The experimental and numerical modes of 9.77  
505 Hz and 9.66 Hz (Figs. 13(a) and 14(a)), 11.72 Hz and 12.09 Hz (Figs. 13(b) and 14(c)) and  
506 14.06 Hz and 13.85 Hz (Figs. 13(c) and 14(d)) show a clear correspondence, which provides a  
507 reasonable level of confidence in the experimental results from the FDD algorithm. Given the  
508 difficulties associated with accurately modelling the real experimental situation, the differences  
509 in the frequencies between numerical and experimental cases are relatively minor. The  
510 numerical mode of 10.55 Hz (Fig. 14(b)) is not sufficiently excited by the traversing model  
511 vehicle in the experiment to show in the peak selection process in Fig. 12. Of note is the  
512 frequency for the numerical mode in Fig. 14(d). The frequency of 13.85 Hz is the same as the  
513 first natural frequency of a single span simply supported beam case. This is unsurprising as the  
514 piers do not show any deflection in Fig. 14(d), equivalent to pinned supports.

515 **Extraction of mode shapes for scoured case**



516

517 Fig. 15: First mode shape (derived from experimental accelerations) for different scour scenarios for vehicle  
 518 crossing at speed of 1.26 m/s (with a tractor mass of 22.7 kg) – (a) Healthy case, (b) 24.5 % stiffness loss at Pier  
 519 2, (c) 24.5 % stiffness loss at Pier 3

520 Fig. 15 shows how the first mode shape of the experimental bridge changes for the scour  
 521 scenarios equivalent to 24.5% stiffness loss at Pier 2 (with other piers remaining healthy) and  
 522 24.5% foundation stiffness loss at Pier 3 (with the other piers remaining healthy). For each  
 523 case, the change in mode shape amplitude is greatest at the location of the scoured pier. Table  
 524 3 shows the MNMS values which are defined in Eq. (2) for the scenarios in Fig. 15. The MNMS  
 525 value at the scoured pier increases due to scour stiffness loss while the MNMS values at the  
 526 other piers decrease. This generally corroborates the findings from the numerical study in a  
 527 previous section. Moreover, the percentage increases in the MNMS values are greater for the  
 528 case of scour at Pier 3 than at Pier 2 - 0.93 to 2.78 (198.9% increase) vs 1.47 to 2.93 (99.3%

529 increase). This is in line with the findings from the numerical study in that the MNMS value  
530 increases more for stiffness loss at an off-centre pier than at the central pier.

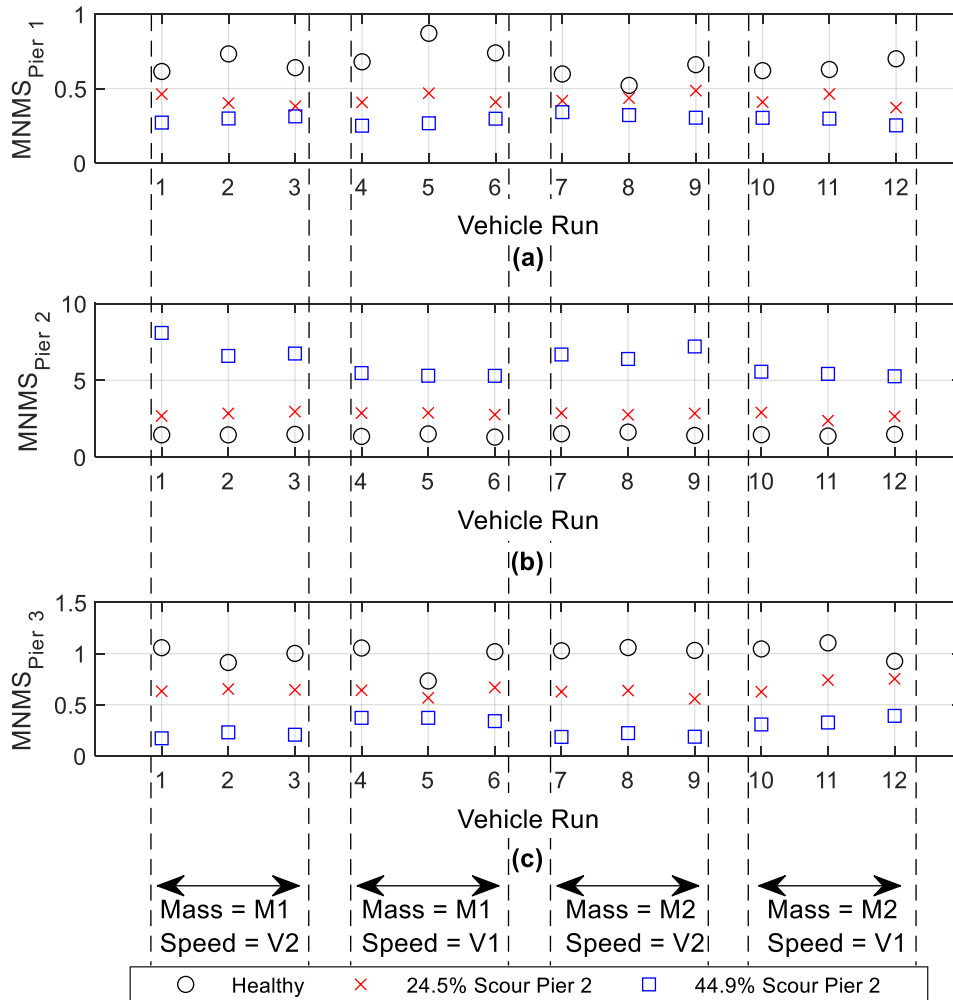
531 Table 3: Experimental MNMS values calculated for 24.5% stiffness reduction (using values marked in Fig. 15)

<b>Scour Condition</b>	<b>MNMS<sub>Pier 1</sub></b>	<b>MNMS<sub>Pier 2</sub></b>	<b>MNMS<sub>Pier 3</sub></b>
Healthy	0.70	1.47	0.93
24.5% Scour Pier 2	0.39	2.93	0.64
24.5% Scour Pier 3	0.32	0.77	2.78

532

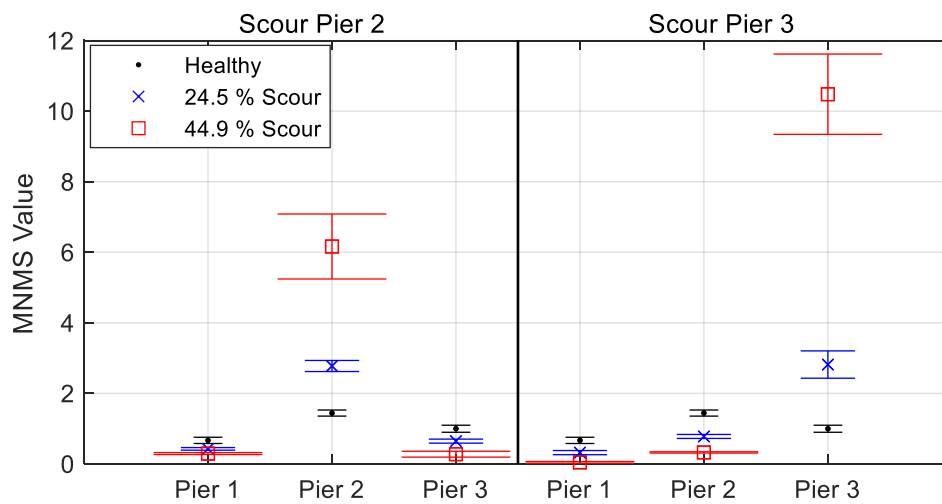
533 **Sensitivity of MNMS for different locations and severities of scour**  
534 **considering vehicle condition variability**

535 Fig. 16 shows the MNMS values for scour at Pier 2 calculated from different vehicle runs for  
536 a healthy case and stiffness losses due to scour of 24.5% and 44.9%. Two different tractor  
537 masses and vehicle speeds are investigated with each repeated three times for each scenario.  
538 The tractor masses tested are 24.3 kg and 26.3 kg, and the vehicle speeds are 1.14 m s<sup>-1</sup> and  
539 1.26 m s<sup>-1</sup>. The MNMS values in Fig. 16 are shown relative to each vehicle run and the specific  
540 conditions are shown below Fig. 16(c). The MNMS values are quite repeatable for each scour  
541 case. This is not unexpected, as the indicators are based on a vibration mode of the structure,  
542 so they should not be significantly affected by a change in vehicle parameters. The results for  
543 the case considered (scour at Pier 2) show that the MNMS increases in value at the scoured  
544 pier for the two scour magnitudes considered and decreases at the remaining piers (relative to  
545 the healthy case).



546

547 Fig. 16: MNMS values for scour at Pier 2 repeated for multiple vehicle runs where M1 and M2 refer to tractor  
 548 masses of 24.3 kg and 26.3 kg respectively and V1 and V2 refer to vehicle speeds of 1.14 m/s and 1.26 m/s  
 549 respectively (a)  $MNMS_{Pier1}$  (b)  $MNMS_{Pier2}$  (c)  $MNMS_{Pier3}$



550

551 Fig. 17: Mean and one standard deviation error bar plots of scour scenarios at Pier 2 and Pier 3 for severities of  
 552 24.5% and 44.9%

553 Fig. 17 (left side) shows the mean of the MNMS values for the 12 runs considered in Fig. 16  
554 +/- one standard deviation (shown by error bars on the plot). The same information is shown  
555 on the right side of the plot for the case where the scour is at Pier 3. There is a clear distinction  
556 between the regions defined by the error bars for each scour scenario. In other words, the error  
557 bars do not overlap, which shows that the effect of scour outweighs any variability effects  
558 (within 1 standard deviation) due to the vehicle changes considered or natural variability due  
559 to measurement error. It can also be seen in Fig. 17 that the scale of the increases at the scoured  
560 pier are far greater than the changes at the unscoured piers, making it clear which pier is scoured  
561 for a given case. Similar to the findings in the numerical study, the MNMS experiences a  
562 greater increase for off-centre piers than for central piers. This is shown in Fig. 17 for the 44.9%  
563 scour case where there is a larger change in MNMS at Pier 3 for the case of scour at Pier 3 than  
564 the change in the MNMS at Pier 2 for the case of scour at Pier 2.

### 565 **Performance of MNMS against Modal Assurance Criterion (MAC)**

566 The performance of the MNMS approach against traditional damage-detection methods based  
567 on comparing healthy and damaged mode shapes using MAC is of interest. In this section, a  
568 brief analysis is conducted to assess the relative performance of MNMS and MAC as indicators  
569 of scour damage. The experimental results from vehicles crossing the model bridge are used to  
570 derive the mode shapes for the case of the healthy bridge, and the bridge 'damaged' by scour  
571 with stiffness reductions of 24.5% and 44.9% at Pier 2. In total, six crossings of the healthy  
572 case, and six crossings for each of the two damage cases are used to obtain the mean values of  
573 the mode shapes for each condition. MAC is defined as in Eq. (7)

$$\text{MAC} = \frac{|\Phi_{\text{healthy}}^t \Phi_{\text{damaged}}|^2}{|\Phi_{\text{healthy}}^t \Phi_{\text{healthy}}| |\Phi_{\text{damaged}}^t \Phi_{\text{damaged}}|} \quad (7)$$

574 where  $\Phi_{\text{healthy}}$  is the mode shape obtained from the healthy bridge,  $\Phi_{\text{damaged}}$  is the mode  
 575 shape obtained from the scoured bridge and "t" defines the matrix transpose. If the mode shapes  
 576 are identical, the MAC will have a value of one, but if they are very different, the MAC value  
 577 will be close to zero.

578 Table 4 shows the results of the MAC analysis. A MAC value of 0.9 between healthy and  
 579 damaged mode shapes is obtained for the case of 24.5% scour-related stiffness loss at Pier 2.  
 580 This reduces to 0.71 for an increased stiffness reduction to 44.9% at Pier 2. Table 5 shows the  
 581 MNMS derived for the same conditions. For 24.5% scour at P2, MNMS at P2 increases by  
 582 almost 100%, and decreases by 41% and 34% at P1 and P3 respectively. For 44.9% scour at  
 583 P2, MNMS at P2 increases by almost 341%, and decreases by 61% and 71% at P1 and P3  
 584 respectively relative to the zero scour case. From this analysis, it can be seen that MNMS is  
 585 more sensitive to scour damage than MAC, and moreover the location of scour can be detected  
 586 by observing the relative changes in the MNMS value at each pier. MNMS is potentially a  
 587 better indicator than the traditional MAC value for scour type damage detection.

588 Table 4 MAC Analysis

	Modal Amplitudes (-)			
Case	Pier 1	Pier 2	Pier 3	MAC
Healthy	-0.23	-0.36	-0.28	-
24.5% Scour	-0.14	-0.45	-0.19	0.9
44.9% Scour	-0.10	-0.62	-0.10	0.71

589

590 Table 5 MNMS Analysis

Case	MNMS <sub>P1</sub>	% Change	MNMS <sub>P2</sub>	% Change	MNMS <sub>P3</sub>	% Change
Healthy	0.71	-	1.41	-	0.96	-
24.5% Scour	0.42	-41	2.82	100	0.63	-34
44.9% Scour	0.28	-60	6.24	341	0.28	-71

591

## 592 **Conclusions**

593 This paper presents an approach to detect stiffness loss arising due to scour based on relative  
594 changes of vertical pier mode shape amplitudes. The method is tested using a scaled  
595 experimental model of a bridge traversed by a vehicle. The experimental mode shapes are  
596 extracted from acceleration signals arising due to the vehicle crossing using an output only  
597 modal identification technique, namely Frequency Domain Decomposition. A scour  
598 monitoring feature (MNMS) is defined, based on the first global mode shape of the structure  
599 and is shown to increase significantly at a scoured pier. At the location of the scoured pier the  
600 magnitude of the MNMS also increases with scour severity, suggesting that progressive scour  
601 development could potentially be monitored. As the algorithm used is an output-only one, it  
602 has the advantage of negating the requirement of knowing any details about the vehicle  
603 excitation forces. Furthermore, material and geometrical information about the bridge such as  
604 second moment of area or density, do not need to be known in order to apply the method.  
605 Repeated vehicle runs to excite the bridge allow the MNMS to be derived and monitoring  
606 changes in this metric alone can potentially detect scour. In practice, an initial visual inspection  
607 of the bridge may help to determine the scour condition at the time of instrumentation, and this  
608 would be the benchmarked ‘unscoured’ case. Once instrumented, the bridge can potentially be  
609 monitored on a continual basis using the method proposed in this paper.

610 It should be noted that while scour is the target damage in the present study, other forms of  
611 damage such as concrete spalling or corrosion will also lead to changes in stiffness of a  
612 structure. Separating the scour influence from other damage types is challenging, however by  
613 the very nature of scour occurring at supports, the relative changes in stiffness due to scour are  
614 expected to be larger than would arise under other damage types. Additionally, if the MNMS  
615 were to detect some form of stiffness loss (from scour or otherwise), this could be used to  
616 trigger a manual visual inspection. It is therefore not so important to separate scour from other

617 damage as the end result for a bridge manager is to detect any issues arising in the structure to  
618 facilitate the safe management of the asset.

619 The analysis in this paper considers scour at only one pier at a time to demonstrate the approach.  
620 Scour at multiple piers simultaneously can cause issues with the method as it is derived using  
621 the sum of the modal amplitudes at all piers to identify scour at a given affected pier. The  
622 method therefore does not work well when scour affects multiple piers of a bridge  
623 simultaneously. However, due to asymmetry in water-flow characteristics across a river  
624 channel cross-section, it is unlikely for temporal scour development to be equal at multiple  
625 piers, therefore the approach should still be capable of identifying scour occurrence once it  
626 begins at a given pier.

627 While the approach was successfully demonstrated with an experimental scaled bridge in the  
628 present study, a full-scale deployment is recommended before firm conclusions on the efficacy  
629 of the method can be made. This is due to the natural differences that arise between 1g scaled  
630 experimental testing and full-scale applications.

631 The approach described in this paper is novel in terms of bridge scour detection and will be  
632 beneficial to the evolving vibration-based scour monitoring field.

### 633 **Data Availability Statement**

634 Some or all data, models, or code that support the findings of this study are available from the  
635 corresponding author upon reasonable request. (Experimental Data.)

### 636 **Acknowledgements**

637 The authors wish to acknowledge the financial support received from Science Foundation  
638 Ireland under the US-Ireland Research Partnership Scheme, Grant No. 14/US/I3033.

639 **References**

- 640 Allemang, R. J. & D. L. Brown. 1982. "A correlation coefficient for modal vector analysis".  
641 *Proceedings of the 1st International Modal Analysis Conference*, 110-116.
- 642 Bao, T. & Z. Liu. 2017. "Vibration-based bridge scour detection: A review". *Structural*  
643 *Control and Health Monitoring*, 24(7), e1937.
- 644 Bao, T., R. A. Swartz, S. Vitton, Y. Sun, C. Zhang & Z. Liu. 2017. "Critical insights for  
645 advanced bridge scour detection using the natural frequency". *Journal of Sound and*  
646 *Vibration*, 386, 116-133.
- 647 Briaud, J. L., S. Hurlebaus, K. A. Chang, C. Yao, H. Sharma, O. Y. Yu, C. Darby, B. E. Hunt  
648 & G. R. Price, 2011. *Realtime monitoring of bridge scour using remote monitoring*  
649 *technology*, Texas A&M University System, Texas.
- 650 Briaud, J. L., Z. Medina-Cetina, S. Hurlebaus, M. Everett, S. Tucker, N. Yousefpour & R.  
651 Arjwech, 2012. *Unknown foundation determination for scour*, Texas Transportation  
652 Institute, Texas.
- 653 Brincker, R., L. Zhang & P. Andersen. 2001. "Modal identification of output-only systems  
654 using frequency domain decomposition". *Smart Materials and Structures*, 10(3), 441-  
655 445.
- 656 Carden, E. P. & P. Fanning. 2004. "Vibration based condition monitoring: a review".  
657 *Structural Health Monitoring*, 3(4), 355-377.
- 658 Chen, C. C., W. H. Wu, F. Shih & S. W. Wang. 2014. "Scour evaluation for foundation of a  
659 cable-stayed bridge based on ambient vibration measurements of superstructure".  
660 *NDT & E International*, 66, 16-27.
- 661 Clough, R. W. & J. Penzien 1993. *Dynamics of Structures*, McGraw-Hill.

- 662 Davis, N. T., E. Hooamaan, M. Sanayei, A. K. Agrawal & F. Jalinoos. 2018. "Integrated  
663 Superstructure-Substructure Load Rating for Bridges with Foundation Movements".  
664 *Journal of Bridge Engineering*, 23(5), 04018022.
- 665 Dos Santos, J. A., C. M. Soares, C. M. Soares & H. Pina. 2000. "A damage identification  
666 numerical model based on the sensitivity of orthogonality conditions and least squares  
667 techniques". *Computers & Structures*, 78(1-3), 283-291.
- 668 Elsaid, A. & R. Seracino. 2014. "Rapid assessment of foundation scour using the dynamic  
669 features of bridge superstructure". *Construction and Building Materials*, 50, 42-49.
- 670 Fan, W. & P. Qiao. 2011. "Vibration-based damage identification methods: a review and  
671 comparative study". *Structural Health Monitoring*, 10(1), 83-111.
- 672 FEMA, 2000. *Prestandard and commentary for the seismic rehabilitation of buildings -*  
673 *Report FEMA-356*, Washington, DC.
- 674 Fitzgerald, P. C., A. Malekjafarian, B. Bhowmik, L. J. Prendergast, P. Cahill, C. W. Kim, B.  
675 Hazra, V. Pakrashi & E. J. OBrien. 2019a. "Scour Damage Detection and Structural  
676 Health Monitoring of a Laboratory-Scaled Bridge Using a Vibration Energy  
677 Harvesting Device". *Sensors*, 19(11), 2572.
- 678 Fitzgerald, P. C., A. Malekjafarian, D. Cantero, E. J. OBrien & L. J. Prendergast. 2019b.  
679 "Drive-by scour monitoring of railway bridges using a wavelet-based approach".  
680 *Engineering Structures*, 191, 1-11.
- 681 Forde, M., D. Mccann, M. Clark, K. Broughton, P. Fenning & A. Brown. 1999. "Radar  
682 measurement of bridge scour". *NDT & E International*, 32(8), 481-492.
- 683 Foti, S. & D. Sabia. 2010. "Influence of foundation scour on the dynamic response of an  
684 existing bridge". *Journal of Bridge Engineering*, 16(2), 295-304.
- 685 Frýba, L. & M. Pirner. 2001. "Load tests and modal analysis of bridges". *Engineering*  
686 *Structures*, 23(1), 102-109.

- 687 Hamill, L. 1999. *Bridge Hydraulics*, Routledge, London & New York, E.& F.N. Spon.
- 688 Hardin, B. O. & V. P. Drnevich. 1972. "Shear Modulus and Damping in Soils: Design  
689 Equations and Curves". *Journal of the Soil Mechanics and Foundations Division*,  
690 98(7), 667-692.
- 691 Ju, S. 2013. "Determination of scoured bridge natural frequencies with soil–structure  
692 interaction". *Soil Dynamics and Earthquake Engineering*, 55, 247-254.
- 693 Keenahan, J., E. J. OBrien, P. J. Mcgetrick & A. Gonzalez. 2013. "The use of a dynamic  
694 truck-trailer drive-by system to monitor bridge damping". *Structural Health  
695 Monitoring*, 13(2), 143-157.
- 696 Khatibi, M., M. Ashory, A. Malekjafarian & R. Brincker. 2012. "Mass–stiffness change  
697 method for scaling of operational mode shapes". *Mechanical Systems and Signal  
698 Processing*, 26, 34-59.
- 699 Klinga, J. V. & A. Alipour. 2015. "Assessment of structural integrity of bridges under  
700 extreme scour conditions". *Engineering Structures*, 82, 55-71.
- 701 Kong, X. & C. S. Cai. 2016. "Scour Effect on Bridge and Vehicle Responses under Bridge–  
702 Vehicle–Wave Interaction". *Journal of Bridge Engineering*, 21(4), Article ID  
703 04015083.
- 704 Kong, X., C. S. Cai & S. Hou. 2013. "Scour effect on a single pile and development of  
705 corresponding scour monitoring methods". *Smart Materials and Structures*, 22(5),  
706 Article ID 055011.
- 707 Kong, X., C. S. Cai & J. Hu. 2017. "The state-of-the-art on framework of vibration-based  
708 structural damage identification for decision making". *Applied Sciences*, 7(5), 497.
- 709 Kwon, Y. W. & H. Bang 2000. *The finite element method using MATLAB*, Boca Raton,  
710 Florida, CRC press.

- 711 Maddison, B. 2012. "Scour failure of bridges". *Proceedings of the Institution of Civil*  
712 *Engineers-Forensic Engineering*, 165(1), 39-52.
- 713 Malekjafarian, A. & E. J. OBrien. 2014. "Identification of bridge mode shapes using short  
714 time frequency domain decomposition of the responses measured in a passing  
715 vehicle". *Engineering Structures*, 81, 386-397.
- 716 Malekjafarian, A. & E. J. OBrien. 2017. "On the use of a passing vehicle for the estimation of  
717 bridge mode shapes". *Journal of Sound and Vibration*, 397, 77-91.
- 718 Moughty, J. J. & J. R. Casas. 2017. "A state of the art review of modal-based damage  
719 detection in bridges: Development, challenges, and solutions". *Applied Sciences*, 7(5),  
720 510.
- 721 Mylonakis, G., S. Nikolaou & G. Gazetas. 2006. "Footings under seismic loading: Analysis  
722 and design issues with emphasis on bridge foundations". *Soil Dynamics and*  
723 *Earthquake Engineering*, 26(9), 824-853.
- 724 OBrien, E. J., P. C. Fitzgerald, A. Malekjafarian & E. Sevillano. 2017. "Bridge damage  
725 detection using vehicle axle-force information". *Engineering Structures*,  
726 153(Supplement C), 71-80.
- 727 OBrien, E. J. & A. Malekjafarian. 2016. "A mode shape-based damage detection approach  
728 using laser measurement from a vehicle crossing a simply supported bridge".  
729 *Structural Control and Health Monitoring*, 23(10), 1273-1286.
- 730 Oztoprak, S. & M. Bolton. 2013. "Stiffness of sands through a laboratory test database".  
731 *Géotechnique*, 63(1), 54-70.
- 732 Pais, A. & E. Kausel. 1988. "Approximate formulas for dynamic stiffnesses of rigid  
733 foundations". *Soil Dynamics and Earthquake Engineering*, 7(4), 213-227.
- 734 Pandey, A., M. Biswas & M. Samman. 1991. "Damage detection from changes in curvature  
735 mode shapes". *Journal of Sound and Vibration*, 145(2), 321-332.

- 736 Prendergast, L. J. & K. Gavin. 2014. "A review of bridge scour monitoring techniques".  
737 *Journal of Rock Mechanics and Geotechnical Engineering*, 6(2), 138-149.
- 738 Prendergast, L. J. & K. Gavin. 2016. "A comparison of initial stiffness formulations for  
739 small-strain soil–pile dynamic Winkler modelling". *Soil Dynamics and Earthquake*  
740 *Engineering*, 81, 27-41.
- 741 Prendergast, L. J., K. Gavin & D. Hester. 2017. "Isolating the location of scour-induced  
742 stiffness loss in bridges using local modal behaviour". *Journal of Civil Structural*  
743 *Health Monitoring*, 7(4), 483-503.
- 744 Prendergast, L. J., D. Hester & K. Gavin. 2016a. "Determining the presence of scour around  
745 bridge foundations using vehicle-induced vibrations". *Journal of Bridge Engineering*,  
746 21(10), Article ID 04016065.
- 747 Prendergast, L. J., D. Hester & K. Gavin, 2016b. Development of a vehicle-bridge-soil  
748 dynamic interaction model for scour damage modelling. *Shock and Vibration*. DOI:  
749 10.1155/2016/7871089
- 750 Prendergast, L. J., D. Hester, K. Gavin & J. O’Sullivan. 2013. "An investigation of the  
751 changes in the natural frequency of a pile affected by scour". *Journal of Sound and*  
752 *Vibration*, 332(25), 6685-6702.
- 753 Prendergast, L. J., M. P. Limongelli, N. Ademovic, A. Anzlin, K. Gavin & M. A. Zanini.  
754 2018. "Structural Health Monitoring for Performance Assessment of Bridges under  
755 Flooding and Seismic Actions". *Structural Engineering International*, 28(3), 296-307.
- 756 Ratcliffe, C. P. 2000. "A frequency and curvature based experimental method for locating  
757 damage in structures". *Journal of Vibration and Acoustics*, 122(3), 324-329.
- 758 Salawu, O. S. & C. Williams. 1995. "Bridge assessment using forced-vibration testing".  
759 *Journal of Structural Engineering*, 121(2), 161-173.

- 760 Scozzese, F., L. Ragni, E. Tubaldi & F. Gara. 2019. "Modal properties variation and collapse  
761 assessment of masonry arch bridges under scour action". *Engineering Structures*, 199,  
762 109665.
- 763 Sohn, H. 2006. "Effects of environmental and operational variability on structural health  
764 monitoring". *Philosophical Transactions of the Royal Society A: Mathematical,*  
765 *Physical and Engineering Sciences*, 365(1851), 539-560.
- 766 Sohn, H., C. R. Farrar, F. M. Hemez, D. D. Shunk, D. W. Stinemates, B. R. Nadler & J. J.  
767 Czarnecki. 2003. "A review of structural health monitoring literature: 1996–2001".  
768 *Los Alamos National Laboratory, USA*.
- 769 Wahab, M. A. & G. De Roeck. 1999. "Damage detection in bridges using modal curvatures:  
770 application to a real damage scenario". *Journal of Sound and Vibration*, 226(2), 217-  
771 235.
- 772 Wardhana, K. & F. C. Hadipriono. 2003. "Analysis of recent bridge failures in the United  
773 States". *Journal of Performance of Constructed Facilities*, 17(3), 144-150.
- 774 Xiong, W., C. Cai, B. Kong, P. Tang & J. Ye. 2018a. "Identification of bridge scour depth by  
775 tracing dynamic behaviors of superstructures". *KSCE Journal of Civil Engineering*,  
776 22(4), 1316-1327.
- 777 Xiong, W., C. Cai, B. Kong, X. Zhang & P. Tang. 2019. "Bridge Scour Identification and  
778 Field Application Based on Ambient Vibration Measurements of Superstructures".  
779 *Journal of Marine Science and Engineering*, 7(5), 121.
- 780 Xiong, W., B. Kong, P. Tang & J. Ye. 2018b. "Vibration-Based Identification for the  
781 Presence of Scouring of Cable-Stayed Bridges". *Journal of Aerospace Engineering*,  
782 31(2), 04018007.

- 783 Zhang, H., S. Chen & F. Liang. 2017. "Effects of scour-hole dimensions and soil stress  
784 history on the behavior of laterally loaded piles in soft clay under scour conditions".  
785 *Computers and Geotechnics*, 84, 198-209.
- 786 Zhu, X. Q. & S. S. Law. 2002. "Moving loads identification through regularization". *Journal*  
787 *of Engineering Mechanics*, 128(9), 989-1000.
- 788